Science of the Total Environment xxx (xxxx) 168342

Contents lists available at ScienceDirect

Science of the Total Environment

journal homepage: www.elsevier.com

Contrasting lake changes in Tibet revealed by recent multi-modal satellite observations

Jiangjun Ran [a], Lin Liu [b], Guoqing Zhang [c], C.K. Shum [d, e], Jiahui Qiu [a], Ruigang Hu [a], Jianping Li [f, g], Junhuan Peng [h, *], Cheinway Hwang [i], Yi Luan [a, *], Yue Sun [f, g], Min Xu [j], Dingmei Chen [k], Jun Ding [a], Yulong Zhong [l]

[a] Department of Earth and Space Sciences, Southern University of Science and Technology, Shenzhen, China
[b] Earth System Science Programme, Faculty of Science, The Chinese University of Hong Kong, Hong Kong, China
[c] State Key Laboratory of Tibetan Plateau Earth System Science, Environment and Resources (TPESER), Institute of Tibetan Plateau Research, Chinese Academy of Sciences, Beijing, China
[d] Division of Geodetic Science, School of Earth Sciences, Ohio State University, Columbus, OH, USA
[e] State Key Laboratory of Geodesy and Earth's Dynamics, Innovation Academy for Precision Measurement Science and Technology, Chinese Academy of Sciences, Wuhan, China
[f] Frontiers Science Center for Deep Ocean Multispheres and Earth System (FDOMES), Key Laboratory of Physical Oceanography, Academy of the Future Ocean, College of Oceanic and Atmospheric Science, Ocean University of China, Qingdao, China
[g] Laboratory for Ocean Dynamics and Climate, Pilot Qingdao National Laboratory for Marine Science and Technology, Qingdao, China
[h] School of Land Science and Technology, China University of Geosciences, Beijing, China
[i] Department of Civil Engineering, National Yang Ming Chiao Tung University, Hsinchu, Taiwan
[j] State Key Laboratory of Cryospheric Science, Northwest Institute of Eco-Environment and Resources, Chinese Academy of Sciences, Lanzhou, China
[k] Shannan Meteorological Service of Tibet, Shannan, China
[l] School of Geography and Information Engineering, China University of Geosciences (Wuhan), Wuhan, China

ARTICLE INFO

Editor: Ouyang Wei

Keywords:
Lake area
Summer expansion
Deep learning
Acceleration
Field campaign

ABSTRACT

The limited anthropogenic activities on the Tibetan Plateau make this an ideal natural laboratory to elucidate how climate change impacts lake changes. Previous studies have mainly focused on decadal lake changes, yet their rapid evolutions at short temporal intervals and the associated atmospheric origins remain elusive. Here, we produce a new lake area change dataset at monthly sampling over 2015–2020 from 16,801 satellite images. Our estimates achieve an accuracy of <30 m, as evidenced by in-situ GPS field survey validations of representative lake shorelines. We found contrasting patterns in recent rapid area changes: deaccelerating in the north and accelerating in the south. Such contrasting pattern was unprecedented in the last two decades and is likely caused by recent precipitation anomalies, indicating that lakes in TP may experience a tipping point. Lakes are found to store only a small portion (<5 %) of net precipitation in summer, increased to ~11 % for years with heavy precipitation, which helps understand the water mass budget for lakes over there. Our study highlights the importance of investigating short-term lake area changes as a climate proxy to study their rapid responses to intra- and inter-annual climate variability.

1. Introduction

The Tibetan Plateau (TP) serves as an excellent natural laboratory for investigating the response of lakes to the ongoing climate change, as there is limited impact from anthropogenic activities due to sparse populations. There are ~1400 lakes, each with an area >1 km^2 the TP (Ma et al., 2011; Zhang et al., 2019; Zhao et al., 2022). As a dynamic system, lake area, level, and volume on the Tibetan Plateau quickly respond to global and regional atmospheric circulations, and are therefore important indicators of changes in temperature and precipitation (Chen et al., 2022; Gronewold and Stow, 2014; Smith et al., 2005; Song et al., 2013; Zhang, 2022; Zhang et al., 2017).

Even though global lakes show an overall decreasing trend in lake area (Yao et al., 2023), the lake areas on the TP have predominantly experienced an obvious expansion over recent decades, observed by optical remote sensing data collected by Landsat series and Sentinel-2 satel-

* Corresponding authors.
E-mail addresses: 2006012076@cugb.edu.cn (J. Peng), luany@sustech.edu.cn (Y. Luan).

https://doi.org/10.1016/j.scitotenv.2023.168342
Received 13 August 2023; Received in revised form 2 November 2023; Accepted 3 November 2023
0048-9697/

lite (Ma et al., 2011; Wan et al., 2014; Zhang, 2022; Zhang et al., 2017). However, due to strong and frequent cloud contamination on optical images, previous studies have usually used data collected over the less cloudy winters, therefore limiting their investigations of lake area changes at annual, multi-year, or longer intervals. Consequently, lake area changes at shorter temporal intervals (e.g., sub-annual and monthly), which are crucial, more sensitive, and previously much less studied indicators of the lakes' response to natural climate variability, remain poorly understood. A recent study by Zhang et al. (2020) made an attempt to extract monthly changes in lake area (>50 km², 165 lakes in total) using the support vector machine classification algorithm, purely based on all-weather synthetic aperture radar (SAR) images from Sentinel-1 satellites. However, a close examination of the SAR images shows that the lake shoreline delineation remains difficult or impossible during winters, because of the indistinguishable similarities between the frozen lake surfaces and the surrounding ice/snow-covered land (see Fig. S1 for an example, where the lake shorelines cannot be determined from January–April).

Combining the complementary advantages of the timing shift between poor quality winter SAR images and cloudy summer optical images, provides an opportunity to combine optical and SAR images to extract the changes in lake area at a higher temporal scale, i.e., monthly. Unlike Zhang et al. (2020), we avoid using the problematic winter SAR images by supplementing the observations with clear optical images (Fig. S1). In this way, we study all lakes with an area of >30 km² (total of 204 lakes) at monthly intervals using deep learning. To validate our lake shoreline estimates, we conducted a field campaign to collect highly accurate shoreline positions with Global Positioning System (GPS) for three typical lakes on the Tibetan Plateau (Fig. 1).

In this article, based on the high temporal (monthly) resolution of lake area changes extracted from SAR and optical images, we are then able to investigate: 1) how the lake area responds to climate changes at the monthly scale, particularly for the heaviest rainfall events in 2016–2018 over the last two decades; 2) what is the possible link between the high temporal lake area changes and the recent rapid oscillations of atmospheric circulation; 3) what is the possible maximal capability of lakes to store the net summer precipitation. The results presented in this study provide, for the first time, a better understanding of how Tibetan lakes respond to climate change at higher temporal scales.

2. Methods and data

2.1. Study area

The Tibetan Plateau (TP), known as the “Roof of the World”, has a total lake area of ~50,000 km² (Zhang et al., 2019). Most of the lakes concentrate in the endorheic basins (Fig. 1); thereby the analysis in this study was mainly focused on the inner TP. In general, the lakes have been experiencing area expansion since mid-1990s (Pekel et al., 2016; Song et al., 2013; Wang et al., 2022; Yao et al., 2019; Zhang et al., 2019; Zhang et al., 2020; Zhao et al., 2022).

For simplicity, three lakes on the TP are selected as examples to analyze the performance of lake shorelines extracted in this study against the available in-situ data. For that purpose, we chose three accessible and representative lakes, namely Selin Co (the largest lake in the inner TP), Nam Co (the second-largest lake in the inner TP), and Yamzho Yumco (the largest lake in the southeastern TP) for the validation.

2.2. Satellite images

Optical data from the Landsat-8 and Sentinel-2 satellite missions are utilized in this study to extract the area changes for lakes whose areas are >30 km² (a total of 204 lakes). Landsat-8 is equipped with Operational Land Imager (OLI) and Thermal Infrared Sensor (TIRS). This satellite is capable of mapping the TP with high temporal resolution (16 days) and spatial resolution (~30 m). For this study, 6689 scenes of OLI band-6 (short-wave infrared) images from the Landsat-8 Level 2 data were chosen to delineate the lake shorelines over 2015–2020, except in the summer and early autumn months (i.e., June to October) because of frequent cloud cover. Sentinel-2 is equipped with Multi-Spectral Instrument (MSI) sensors and has been monitoring the TP every 10 days at a spatial resolution of 10 m since 2016. We selected 5910 scenes from MSI band-11 (also short-wave infrared) at the Level 2 processing to obtain the lake area changes over 2016–2020, except for the summer months.

Level 1 Ground Range Detected (GRD) SAR images (4202 scenes) from the Sentinel-1A/B satellites, collected in Interferometric Wide (IW) swath mode during the summer months over 2015–2020, were used to complement the optical images. The nominal spatial resolution of the SAR images is 5 × 20 m. The temporal resolution of Sentinel-1 A/B is 6 days.

2.3. CNN architectures to extract lake area changes

The artificial intelligence-based methods allow water bodies to be identified from remote sensing images (Li et al., 2022; Li et al., 2019; Weng et al., 2020; Yuan and Sarma, 2010; Zhang et al., 2020). When processing the optical images, we used our in-house Convolutional Neural Network (CNN) architecture LaeNet (Liu et al., 2020). For the summer months of 2015–2020, this CNN algorithm is more difficult to apply because of the strong speckle noise in the SAR images and the absence of clear optical images. Therefore, we used CloudNet (Zhang et al., 2018) to process the SAR images obtained in the summer months (Fig. S2).

In months for which optical images were not available, we utilized SAR images instead. As the SAR images are typically noisy, the training process for the CloudNet architecture (Fig. S2) involved the use of SAR images along with some optical images collected during other months (Chen, 2022). In order to reduce the noise in the SAR images, we filtered the SAR images with the Refined Lee filter (Yommy et al., 2015). Then, based on a 1:2 ratio of optical to SAR images, the resampled optical image and the filtered SAR image are merged into a new three-band image. It is also worth mentioning that for complex lakeshores, we introduced buffer zones around the shorelines to manually help with the classification of water and non-water bodies (similar to Zhang et al., 2020). Since the lake shorelines vary from year to year, but generally the buffer zone of the next year is larger than the previous one, we manually updated the buffer zone for each year. Note that the buffer zone referred here is for each lake, and is quite different with the buffer zone considered in the GRACE/GRACE-FO data processing, where it aims to minimize the signal leakage.

It was found that our procedure (see Fig. S2) improved the performance, even though the optical images were not collected in the same month as the SAR images. The recall, accuracy, precision, and mIoU (mean Intersection over Union) for CloudNet were 0.990, 0.983, 0.981, and 0.938, respectively.

In short, we use deep learning (i.e., the CloudNet and LaeNet) to extract the water- and non-water bodies in the buffer zone from the SAR and optical satellite images, and then take boundaries of water- and non-water bodies as the lake shorelines. In this way, the lake area is the summation of two parts: i.e., the constant part of area formed by the inner boundary (see Area_inner in Fig. S3) and the time variable part of area in the buffer zone (see Area_buffer in Fig. S3).

2.4. Satellite gravimetry products

The total terrestrial water storage (TWS) changes over 2015–2020 from satellite gravity missions, i.e., GRACE (the Gravity Recovery and Climate Experiment, Tapley et al., 2019) and its successor GRACE Follow-On (Landerer et al., 2020), are utilized in this study to investigate

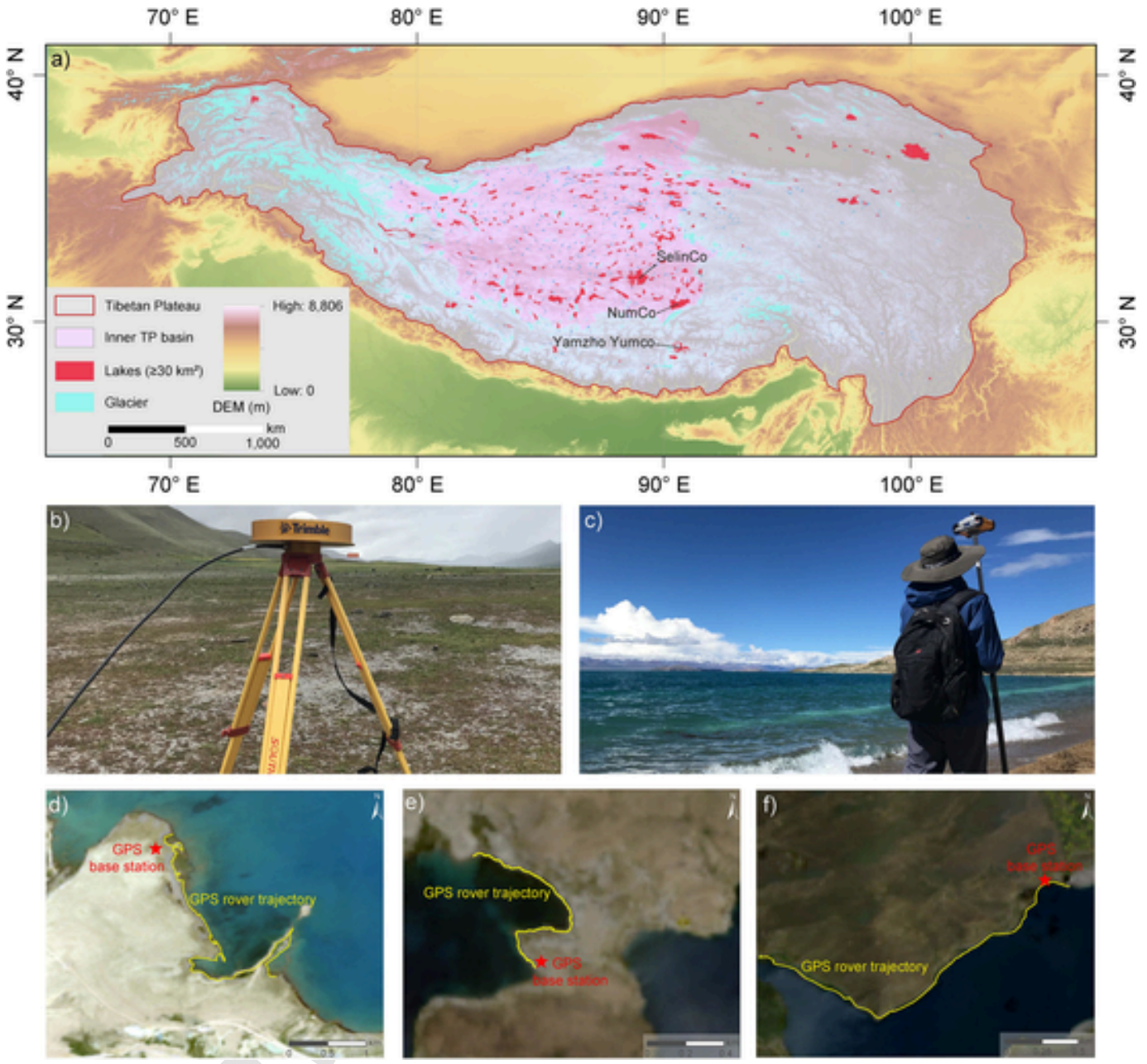

Fig. 1. A field campaign to collect in-situ lake shorelines. a) Distribution of lakes (>30 km²; total number: 204) investigated in this study. The three typical lakes, i.e., Selin Co, Num Co, and Yamzho Yumco, which were selected to conduct the field campaign using GPS, are marked with black arrows. b) GPS base station (red star) used as a high-precision reference when computing the coordinates of the lake shorelines using a GPS rover station. c) GPS rover station held by a moving surveyor away from the water at distances of ~1 m. d) Field campaign for Selin Co on August 20, 2020. The GPS rover trajectory of Selin Co is shown as the yellow line, whereas the GPS base station is indicated as a red star. e) GPS base and rover trajectory for Nam Co on August 2, 2020. f) GPS base and rover trajectory for Yamzho Yumco on July 31, 2020. The Landsat 8 optical images, which are most closed to the field campaign time, are shown as the background in d)-f).

the net mass variations on the Tibetan Plateau. The State-of-The-Art mascon products released by the National Aeronautics and Space Administration, Jet Propulsion Laboratory (JPL RL06.1_v03) (Watkins et al., 2015; Wiese et al., 2016) are considered here. The mascon products are provided at monthly time interval and grided at 0.5-by-0.5° with nominal spatial resolutions of 3-by-3°. In order to account for the signal leakage caused by the coarse spatial resolution of GRACE/GRACE-FO (Ran et al., 2021), a buffer zone with the width of 50 km is introduced, when computing the total mass changes of inner Tibetan Plateau.

By subtracting the surface water storage, canopy water storage, soil moisture storage, snow water equivalent, and glacier dynamics modelled by the ensemble mean of three variants (i.e., Noah, CLM, and VIC) of GLDAS hydrological models, from the total terrestrial water storage from GRACE/GRACE-FO, it is possible to evaluate the modelled ground water from hydrological models (e.g., PCR-GLOBAL, GLDAS) and the derived value from this study.

2.5. Field campaign to collect in-situ lake shorelines by GPS

The lake shorelines delineated from the satellite optical and/or SAR images may contain some misclassified water and non-water bodies (Zhang et al., 2019). To understand the uncertainty level of the extracted lake shorelines, it is important to validate them against independent data. We conducted a field campaign to map the lake shorelines

with high accuracy (i.e., ~10 cm) using GPS. Three typical lakes (i.e., Selin Co, Nam Co, and Yamzho Yumco) are considered in this study. For each lake, we selected one part of the shoreline with a length of ~5 km and obtained its coordinates using GPS (Fig. 1). Because of the complex topography of the TP, the shoreline geometries are quite diverse. Therefore, to make our validation more reliable, we selected shoreline shapes from three different lakes. For instance, the stretch of shoreline recorded at Selin Co is the most complicated, with many sharp turns, whereas that considered at Yamzho Yumco is relatively simple (Fig. 1), with a mostly straight line.

The field campaign was carried out on three days in July and August 2020. For each lake, we first installed a static GPS base station equipped with a Trimble Alloy receiver (Fig. 1). A moving GPS rover station equipped with a SOUTH receiver was held by a surveyor who walked at distances of ~1 m from the lake shoreline. In this way, we were able to obtain coordinates of centimeter-level accuracies using differential GPS.

In this study, the lake shoreline predicted by the deep learning model from satellite images is compared with the in-situ GPS data, and the root mean square error (RMSE) between them is calculated as follows:

$$RMSE = \sqrt{\frac{1}{N}\sum_{i=1}^{N}\left(x_i^{GPS} - x_i^{DL}\right)^2 + \left(y_i^{GPS} - y_i^{DL}\right)^2} \quad (1)$$

where (x_i, y_i) is the coordinate of a lake boundary pixel; (x_i^{DL}, y_i^{DL}) indicates that the pixel is predicted by the deep learning, and (x_i^{GPS}, y_i^{GPS}) indicates that the pixel is the measured GPS boundary data. d_i represents the distance between the predicted boundary point and the measured boundary (x_i^{DL}, y_i^{DL}) and (x_i^{GPS}, y_i^{GPS}).

2.6. Lake level dataset

Lake levels can be monitored with satellite altimetry missions (Arabsahebi et al., 2018; Huang et al., 2018; Xu et al., 2022; Zhang et al., 2011). As the lake area and level typically exhibit a strong correlation on the TP (Zhang et al., 2020), we treated the lake level as independent data for comparing the extracted area changes and investigating the response of lakes to atmospheric oscillations. The lake levels provided by Hydroweb (https://hydroweb.theia-land.fr/), the Global Reservoirs and Lakes Monitor (G-REALM, https://ipad.fas.usda.gov/cropexplorer/ global_reservoir/), and Xu et al. (2022) were used and aggregated in this study. Note that due to limited spatial and temporal resolutions of altimetry data, there are only 36 large lakes with monthly lake level time series available.

2.7. Lake area data processing

After extracting the monthly lake area changes using deep learning, we examined their performance in two independent ways. The first way is to validate using in-situ lake shorelines of representative lakes. The second way is that by following previous studies that inferred a strong correlation between lake area and level, we thereby compared correlation between the time series of extracted lake area and lake levels. Also, in line with Song et al. (2013), we empirically reconstructed the lake level data at the monthly scale for all lakes considered in this study; then the lake area and level data were utilized to compute the lake water mass changes over 2015–2020 and compared with independent GRACE/GRACE-FO mascon product from NASA JPL. Note that the months with missing lake area or level data were interpolated with the regularized expectation–maximization method (Schneider, 2001).

Furthermore, the lake area trend and acceleration over 2015–2020 were calculated by fitting lake area change time series with bias, trend, acceleration, annual, and semi-annual terms (see Eq. 2). We acknowledge that the time span, i.e., 2015–2020, is short to obtain reliable acceleration estimates. Therefore, the acceleration changes in lake area here may likely refer to the transient variations.

$$f(t) = A + B(t - t_0) + \frac{1}{2}Ct^2 + D\sin\omega(t - t_0) + E\cos\omega(t - t_0) + F\sin 2\omega(t - t_0) + G\cos 2\omega(t - t_0) \quad (2)$$

where A to G are coefficients estimated by a least-square estimator. t_0 is the reference time. $\omega = 2\pi/T$, while $T = 1$ year.

In addition, we normalized the lake area time series over 2015–2020, and then grouped them into four categories based on the contrasting pattern of the accelerations (τ) of lake area changes: 1) Decelerating category with $\tau < -0.5$ km²/yr²; 2) Transition category A with $-0.5 < \tau < 0$ km²/yr²; 3) Transition category B with $0 < \tau < 0.5$ km²/yr²; and 4) Accelerating category with $\tau > 0.5$ km²/yr².

Finally, in order to examine the significant summer expansion of lake area, we first estimated the summer area increase (ΔS) for a given year as the difference in mean lake area between autumn and spring. Then, we define the year as having a sharp summer increase if ΔS is at least twice the mean ΔS over 2015–2020.

2.8. Climate data

Precipitation, temperature, and snow depth data for the TP were collected from ERA 5 Land (ERA5L), which is the fifth generation of atmospheric reanalysis of the global climate by the European Centre for Medium-range Weather Forecasts. ERA5L provides daily data gridded at 0.1° × 0.1° (Muñoz-Sabater, 2019). We computed the net monthly precipitation, temperature and snow for the inner TP, and interpolated the monthly precipitation time series for each lake. We also considered other precipitation products, e.g., China Gauge-Based Daily Precipitation Analysis (CGDPA, 0.5° × 0.5°) from China Meteorological Administration (CMA), Global Precipitation Climatology Project (GPCP, 2.5° × 2.5°), and high-resolution precipitation dataset for the Third Polar region (TPHiPr, 1/30° × 1/30°) (Shen and Xiong, 2016; Adler et al., 2018; Jiang et al., 2023). Since our study aims to analyze the area changes at a very high spatial scale, i.e., at the individual lake scale (> 30 km²), therefore we find the high spatial resolution precipitation products from ERA5L (0.1° × 0.1°) or TPHiPr (1/30° × 1/30°) are more suitable for analysis in this paper. In addition, to examine the mass changes by snow, groundwater, soil moisture, and canopy water are obtained by the ensemble mean of three land surface models: NOAH, CLSM, and VIC, provided by of Global Land Data Assimilation System (Rodell et al., 2004).

Furthermore, to understand the driving forcing from atmospheric circulations for the observed lake area changes, we computed the seasonal intensity of normalized surface wind field as Dynamic Normalized Seasonality (DNS) index at 200 hPa (which corresponds to ~12,000 m) within the domain (27° – 35°N, 70° – 95°E) (Li and Zeng, 2003). The hourly wind field data grided at 0.25° × 0.25° were provided by the ERA-5 (Hersbach et al., 2018). In line with the timing of precipitation on the TP, we computed the DNS index by utilizing ERA5L surface wind field output for months from April to September.

3. Results

3.1. Validation of delineated lake shorelines against in-situ GPS data

The lake shorelines were delineated as the boundary of the water and land (see the shorelines of Selin Co, Nam Co, and Yamzho Yumco in Fig. 2). The RMS of the differences between the lake shorelines extracted in this study and those obtained by the in-situ GPS campaign for

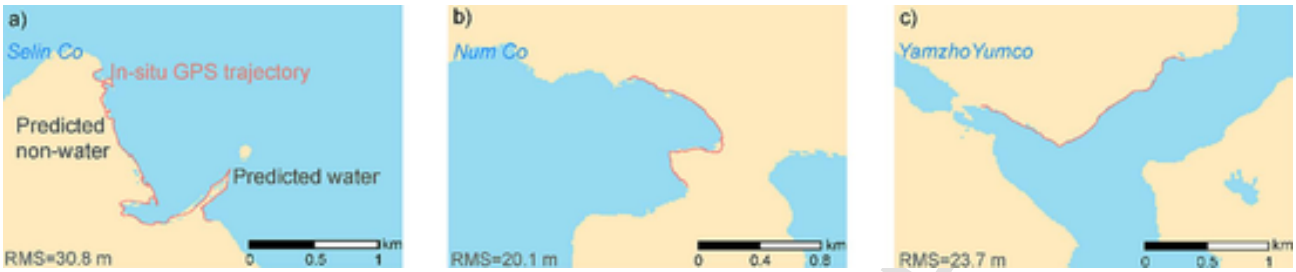

Fig. 2. Deep-learning-based lake shorelines predictions. a) Predicted water and non-water areas for Selin Co determined by deep learning in this study are indicated in blue and yellow, respectively. The in-situ GPS trajectory collected in this study is shown as the red curve. The RMS of the difference between the in-situ GPS trajectory and the shoreline predicted in this study is 30.8 m. b) Similar to a), but for Num Co. c) Similar to a), but for Yamzho Yumco.

Table 1
Statistics of lake shoreline estimates. Field campaign to collect in-situ GPS lake shoreline profiles at three typical lakes to validate the lake shorelines predicted by deep learning in this study.

	Selin Co	Nam Co	Yamzho Yumco
Length of the profile by GPS (km)	10.3	2.9	4.7
RMS of the differences (m)	30.8	20.1	23.7

Selin Co, Nam Co, and Yamzho Yumco are 30.8, 20.1, and 23.7 m, respectively, corresponding to around 1 pixel for Landsat-8 images and 2–3 pixels for Sentinel-2 images (Table 1).

The correlation coefficient between lake area and level is close to 1, with the R^2 value around 0.9 for the three typical lakes considered herein (Fig. 3). We examined the correlation between the monthly lake area time-series from 2015 to 2017 reported by Zhang et al. (2020) and the available monthly lake level time-series (for a total of 25 lakes). We find that the mean correlation coefficient is ~0.36 for the lake area data from Zhang et al. (2020), whereas the mean correlation coefficient is ~0.95 for the lake area data extracted in this study (Fig. S4).

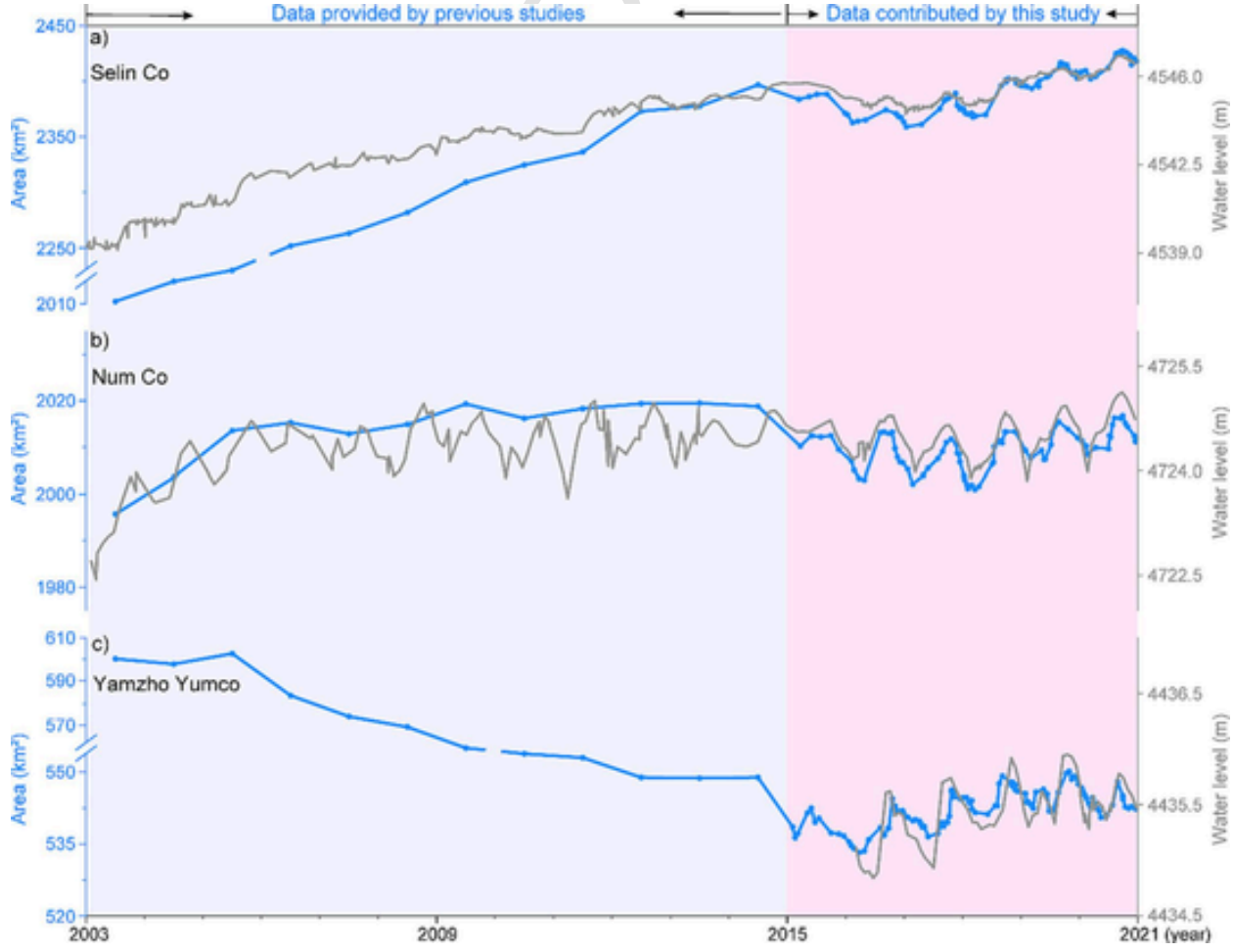

Fig. 3. Extracted lake areas and shorelines in this study. a) Monthly lake area time series for Selin Co over 2015–2020 contributed by this study is shown as the blue line. For comparison, the annual lake area changes over 2003–2014 provided by previous studies are also included. The available water level data are shown as the gray line. b) Similar to a), but for Num Co. c) Similar to a), but for Yamzho Yumco.

The *monthly* lake area data for Selin Co, Nam Co, and Yamzho Yumco are shown in Fig. 3 as examples. The lake area data over 2003–2014 contributed by previous studies (Zhang et al., 2019; Zhao et al., 2022) are also shown. From the rate in lake area data over 2015–2020 (Fig. S5), almost all the lakes (194 out of 204) expanded during this period, with only a few lakes concentrated in the southeastern inner TP decreasing in area. In addition, from Fig. 3a–c, one can also observe obvious sub-annual variations that had not been identified in previous studies.

3.2. Contrasting regional patterns in accelerated lake area changes

The newly-discovered accelerations of lake area changes over 2015–2020 reveal obvious contrasting regional patterns (at the 95 % confidence level) for the lakes in the inner TP (Fig. 4). The largest increasing acceleration of lake area changes was 5.6±0.8 km^2/yr^2 for Selin Co in the southern inner plateau, whereas the largest decreasing one was −6.0±0.7 km^2/yr^2 for Maergai Chaka in the northern inner plateau. Even though almost all the lakes were expanding during this time period (Fig. S5), those in the northern inner plateau clearly exhibited deceleration, whereas those located in the southern inner plateau exhibited significant acceleration (Fig. 4). The central inner plateau is a gradual transition zone. As shown in Fig. 4, similar contrasting regional patterns are also evident in lake level changes.

To investigate whether such contrasting patterns occurred in previous years, we examined the accelerations of lake area changes over the last two previous six-year periods, i.e., 2003–2008 and 2009–2014. For 2003–2008, the lakes in the central inner plateau accelerated in area, whereas those in the northern and southern parts were decelerating (Fig. S6). During 2009–2014, most lakes showed decelerating in lake area changes (Fig. S6), except for a slight accelerating in the southwestern inner plateau. Note that the confidence level of 95 % applies to far fewer lakes (< 23) in the periods 2003–2008 and 2009–2014 than for 2015–2020. This is because the temporal samplings for lake area changes in the two earlier six-year periods were limited to one measurement per year (Zhao et al., 2022) or less (Zhang et al., 2017). The analysis above suggests that the past three six-year periods covering 2003–2020 (roughly two decades) did not exhibit the same pattern in the observed accelerations of the lake area changes in this study.

By examining the acceleration of precipitation products from ERA5L, we infer that the contrasting patterns observed in the lake area data for each period were related to oscillations in local precipitation (Fig. S7). The correlation between lake area and precipitation changes over 2015–2020 is very close to 1 for most lakes. Note that we also examined other possible contributors, e.g., snow, glacier, and temperature. However, we find no clear linkage between them and the lake area acceleration change patterns.

3.3. Significant summer expansion of lake area

Based on the ERA5L precipitation product, there are significant inter- and intra-annual variations. In particular, the summers of 2016, 2017, and 2018 had the heaviest precipitation over the previous ~20 years (Figs. S8 and S9). As shown in Fig. 5, we infer that the decelerating category (Fig. 5a) is caused by the sharp summer increases in lake area in 2016 and 2017, whereas negligible or no increases occurred in the other years. For transition category A, the summer expansion also occurred in 2016 and 2017, but these played a relatively smaller role than in the decelerating category. There was an obvious summer expansion in 2018 as well, but weaker than in 2016 and 2017.

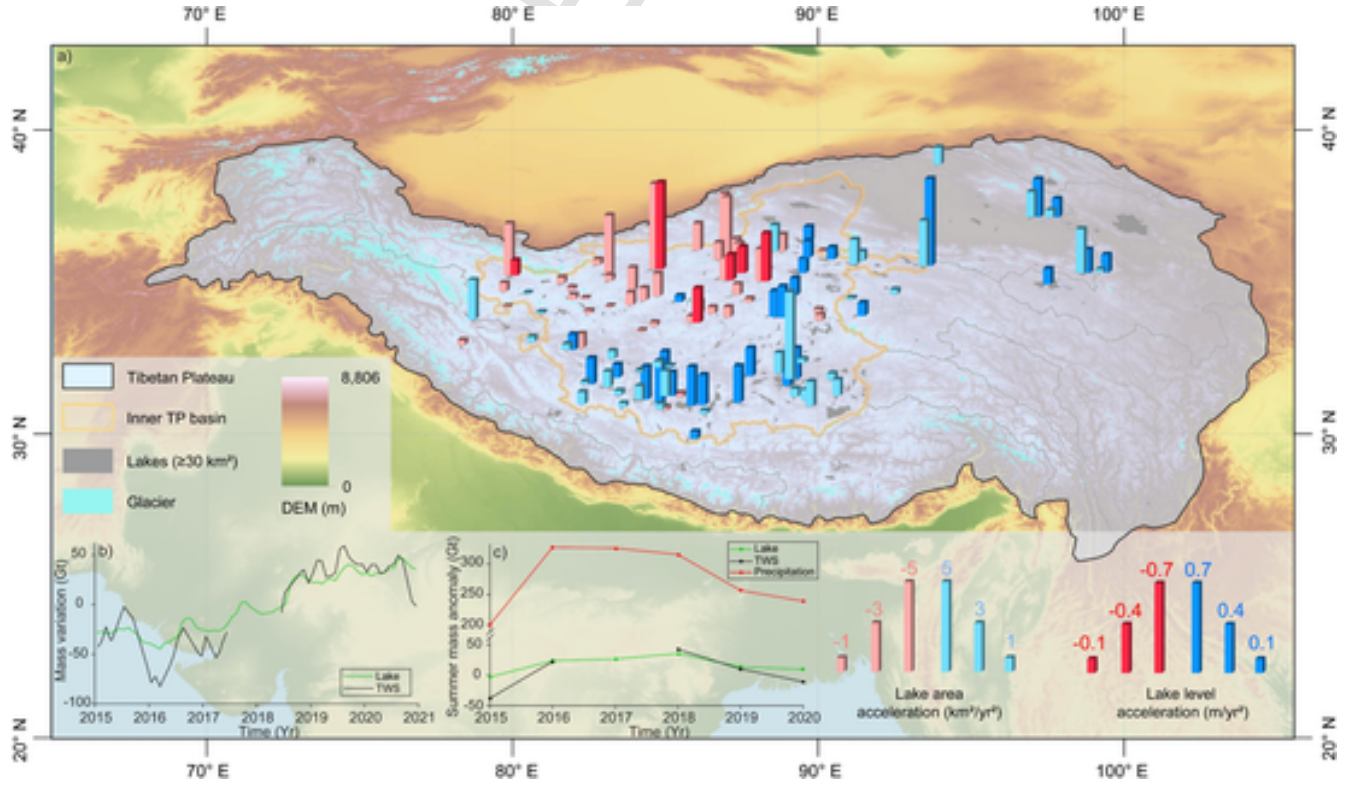

Fig. 4. Contrasting regional patterns of lake area and level acceleration changes. (a) The estimated lake area accelerations and aggregated lake level changes (at the 95 % confidence level) over 2015–2020. Note that the acceleration of lake area and level are indicated with red/blue and light red/blue bars, respectively. Trend over 2015–2020 of annual changes in water level using aggregated data from Hydroweb, G-REALM, and Xu et al. (2022). (b) The net water mass change time-series in lakes on the inner Tibetan Plateau over 2015–2020 is shown in green, whereas the total terrestrial water storage (TWS) of the same area observed by GRACE/GRACE-FO is in black. (c) The summer lake water expansion in mass (Gt) at the yearly interval over 2015–2020 is delineated with the green curve; similarly, the summer net terrestrial water storage and precipitation anomalies are in black and red, respectively.

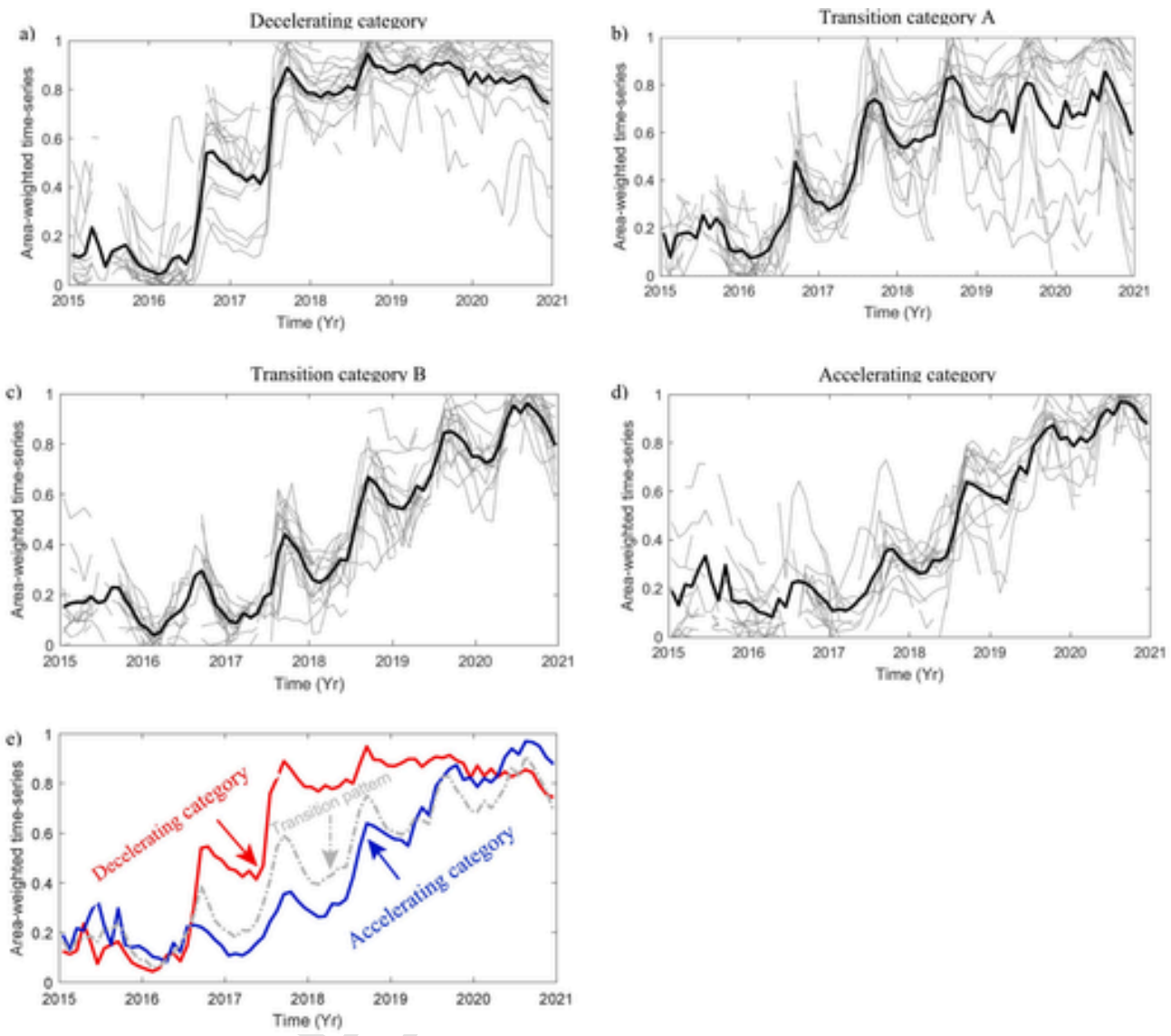

Fig. 5. Normalized lake area time series for different categories. a) Decelerating category with acceleration $\tau < -0.5$ km²/yr². b) Transition category A with $-0.5 < \tau < 0$ km²/yr². c) Transition category B with $0 < \tau < 0.5$ km²/yr². d) Accelerating category with $\tau > 0.5$ km²/yr². Each thin gray line denotes a lake. The thick black line shows the mean of all lakes of each category. e) Combined patterns averaged from each category. Note that we have combined transition categories A and B into a single transition category.

It is worth noting that the strong seasonality of lake area changes in the decelerating category was only presented 8than in 2016 and 2017. It negligible for the remaining years. For the two transition categories and the accelerating category, however, the seasonality was prominent in all years. In transition category B and the accelerating category, the summer expansion in 2018 was larger than that of the other years. Furthermore, there was a continuous increase in lake area from 2018 to 2020 in transition category B and the accelerating category, whereas the lake area remained relatively stable from 2018 to 2020 in the decelerating category and transition category A. In the accelerating category, the lake area in 2015 was slightly larger than in 2016, whereas no such decrease occurred in transition category B.

To better understand the temporal causes for the contrasting acceleration pattern, we examine the geographically averaged normalized lake area change time-series for each category and present them together in Fig. 5e. Note that for simplicity, we have combined transition categories A and B as a single transition category. Corresponding to the three averaged patterns, we chose a representative lake for each pattern to examine the lake shoreline responses from 2015 to 2020. For the accelerating category, it is found that the shoreline of Selin Co retreated slightly in 2016 compared with 2015, followed by a continuous advance from 2017 (Figs. S10–11). For the transition category, a part of the shoreline of Tso Meima ($\tau = 0.1$ km²/yr²) indicated a continuous advance from 2015 to 2020 (Figs. S10–11). For the decelerating category, we chose a part of the shoreline of Maergai Chaka. The lake shoreline exhibited a sharp advance in 2016 and 2017, whereas it remained unchanged in the subsequent years (Figs. S10–11). These changes in lake shorelines were consistent with the patterns extracted from the time series of lake area changes (Fig. 5).

We also observed sharp summer expansions in 2016 and 2017 (Fig. 5a-b), with a relatively smaller but still obvious summer expansion in 2018 (Fig. 5c-d), in all four categories. As shown in Fig. 6a-f, from 2015 to 2020, the number of lakes in which a sharp summer expansion occurred quickly increased from 2015 to 2016, then reached the maximum in 2016–2018, and finally vanished from 2019 to 2020. Interestingly, it is found that the summer expansion spatially started in the northern inner plateau, and gradually shifted to the southern inner plateau (Fig. 6a-f).

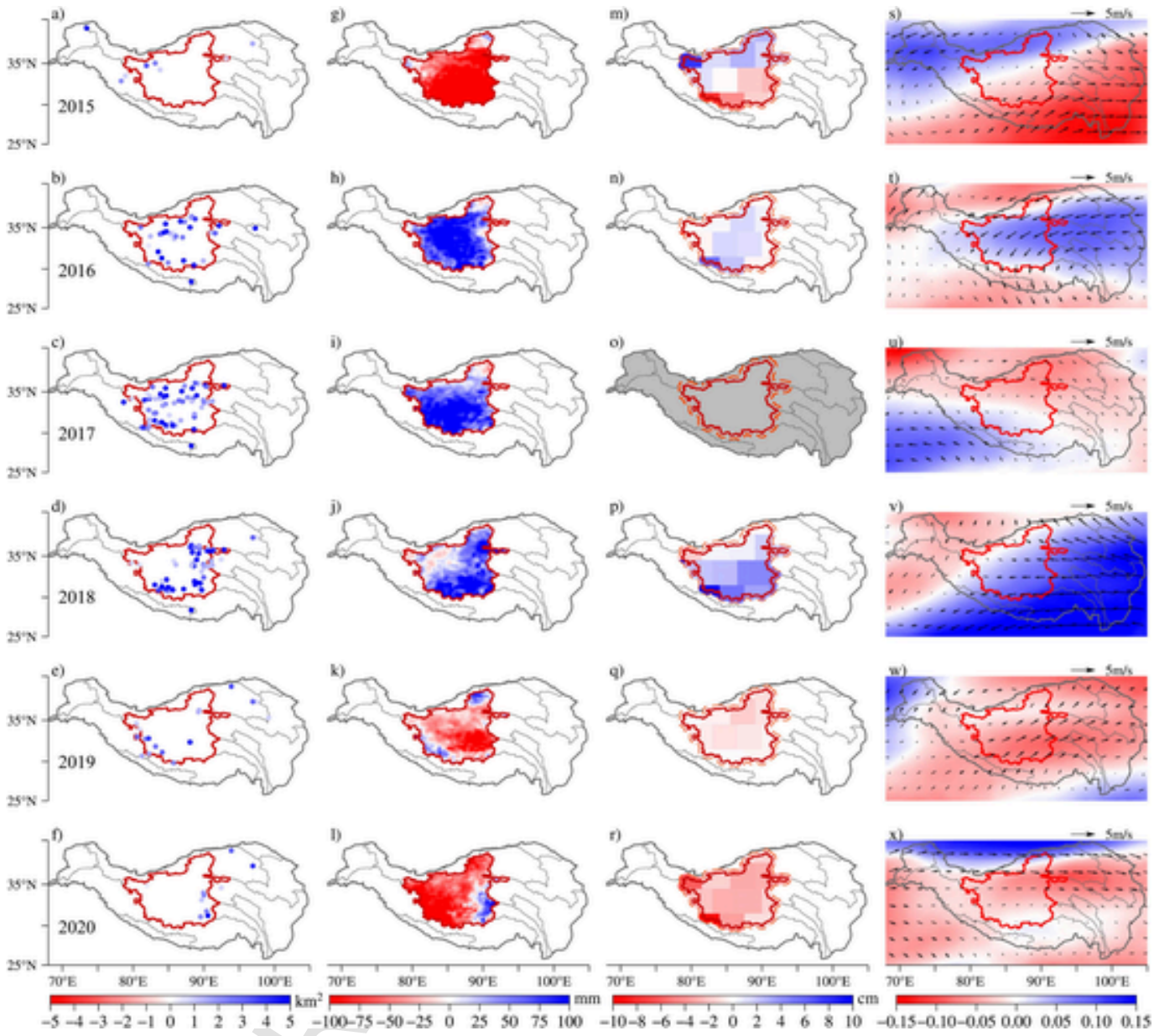

Fig. 6. The Summer expansion for different key climatic factors. Summer expansion in lake areas (a-f), net precipitation anomalies (g-l), total GRACE/FO-based TWS (m-r), and the Dynamic Normalized Seasonality (DNS) and wind (vector, m/s) at 200 hPa (s-x) at annual intervals over 2015–2020. Note that there is no data for TWS in 2017 because of the gap between GRACE and GRACE-FO missions.

3.4. Atmospheric forcing of summer expansion associated with heavy precipitation events

To explore the underlying reasons for this spatiotemporal evolution of lake area changes, we examined the annual net precipitation anomalies for the inner TP. As shown in Fig. 6g-l, the large precipitation anomalies well correspond to the significant summer expansion in lake areas both spatially and temporally. According to the ERA5L precipitation product, the largest net precipitation events over the past 20 years occurred in 2016, 2017, and 2018 (Fig. S8). Furthermore, we examined the responsible driving force of variations in atmospheric circulations over 2015–2020 at a large spatial scale. It is found that in general, the positive DNS index in 2016 (entire inner TP), 2017 (southwestern inner TP) and 2018 (southeastern inner TP) show a good consistency with heavy precipitation occurred in 2016–2018 at the regional spatial scale (Fig. 6s-x). In particular, the "L"-shape precipitation pattern in 2018 (Fig. 6j) was likely associated with wind direction changes from the southeastern inner TP (see the northward and southward wind vector changes in Fig. 6v). Such recent precipitation anomalies in 2016, 2017, and 2018 were likely caused by the weakened westerlies and strengthened south Asian summer monsoon. However, further studies are needed to understand the atmospheric origin.

Furthermore, we also considered how other possible climatic factors contributed to the summer expansion in lake area. As shown in Fig. S12, even though some patterns were observed in the summer anomalies of snow, groundwater, soil moisture, canopy water, and temperature, their patterns showed almost no clear linkage to that of lake area summer expansion. As for the summer glacier changes in the inner Tibetan Plateau, we do not show them here because of their negligible amplitude (Zhang et al., 2020).

3.5. Linkage of lake area summer expansion to TWS anomaly

Interestingly, we examined the summer TWS anomalies from GRACE/GRACE-FO and found that the lake water mass change time series over 2015–2020 was consistent with that of TWS. As shown in Fig. 4b, the long-term trends over 2015–2020 for lake mass and TWS trend were 15 Gt/yr and 17 Gt/yr, indicating ~2 times lake mass gain than the trend (e.g., ~8 Gt/yr) of previous periods (Wang et al., 2016). Furthermore, the summer mass increases in TWS observed by GRACE/GRACE-FO were believed to be caused by the lake water accumulation in summer (Figs. 4c and 6). It is also worth to mentioning that 1) for the heavy precipitation years (i.e., 2016–2018), only ~11 % of the net summer precipitation is stored by the lakes; 2) for the other years, even less (<5 %) water is buffered (see Fig. 4c).

4. Discussion and conclusions

In this study, we have combined optical and SAR images to extract the *monthly* lake area changes 2015–2020 for lakes with each area > 30 km² using deep learning. This significantly improves the temporal resolution of lake area changes compared to previous studies (Ma et al., 2011; Wan et al., 2014; Zhang, 2022; Zhang et al., 2017). By validating the satellite data against in-situ GPS data, we found that the accuracy of the lake shorelines obtained in this study was within 1–2 pixels (<30 m).

By investigating the acceleration of lake area changes over 2015–2020, we identified a statistically significant contrasting regional pattern in the inner TP. This indicates that, although most lakes are expanding, those in the northern inner TP were experiencing a significant deacceleration of lake area changes, whereas an accelerating pattern can be observed for lakes in the southern inner TP, likely caused by recent rapid precipitation anomalies. Other climatic factors such as snow and temperature contributed negligibly to such pattern changes. This contrasting pattern was not presented in the previous ~20 years, which may indicate the lakes experienced a tipping point.

The investigation on mass budget in TP is quite challenging, mainly because of sparse reliable observations over there. This largely limits our understanding of its response to climate changes. However, the inner TP is an excellent natural laboratory because it is an endorheic basin with negligible human impacts, and thereby with a much simpler mass balance condition. By far, several mass balance components for inner TP are still quite uncertain, i.e., surface water storage, groundwater water storage, etc. Here, in this study, using an accurate estimate of the surface water storage, i.e., mainly referring to the lake mass changes extracted in this study, we suggest that ground water storage modelled by the state-of-the-art hydrological models (e.g., PCR-GLOBAL, GLDAS) roughly overestimates the trend and seasonal amplitude by >2 times than that by this study (Fig. S13). This indicates extensive studies are still needed to explore the ground water storage over there.

Furthermore, Lakes are found to store only a small portion (<5 %) of net precipitation in summer, increased to ~11 % for years with heavy precipitation. This indicates a bench mark for water mass budget for inner TP. Our study provides a novel opportunity to investigate the response of lake areas to natural climate variability at intra-annual scales.

Data availability

The monthly Tibetan lake area time series over 2015–2020 can be found at https://zenodo.org/record/8424857. The Sentinel-1 and Sentinel-2 data are downloaded from the European Space Agency. The satellite images of Landsat-8 are downloaded from the U.S. Geological Survey (USGS). The lake area between 2003 and 2014 are available at https://zenodo.org/record/7009755. The lake level data from altimetry are available at https://zenodo.org/record/5732806#.YpcXEajP25c, the Hydroweb (http://hydroweb.theia-land.fr), the Global Reservoir and Lake Monitor database (G-REALM; https://ipad.fas.usda.gov/cropexplorer/global_reservoir) and the National Tibetan Plateau Data Center (http://data.tpdc.ac.cn/). Jet Propulsion Laboratory (JPL) at the National Aeronautics and Space Administration (http://grace.jpl.nasa.gov) is acknowledged for mascon solutions.

Code availability

The codes for processing the satellite images are available from the corresponding authors.

CRediT authorship contribution statement

J.R. designed this study. J.R. and L.L. analyzed the results and wrote the manuscript. J.Q. and R.H. produced the lake area data. All authors commented on the manuscript.

Declaration of competing interest

The contact author has declared that no conflict of interest exits in the submission of this manuscript, and the manuscript is approved by all authors for publication. I would like to declare on behalf of my co-authors that the work described was original research that has not been published previously and not under consideration for publication elsewhere, in whole or in part. All the authors listed have approved the manuscript that is enclosed.

Acknowledgments

We thank the National Natural Science Foundation of China (42322403, 42174096, 41974094) and CUHK Direct Grant For Research (4053481) for their support.

Appendix A. Supplementary data

Supplementary data to this article can be found online at https://doi.org/10.1016/j.scitotenv.2023.168342.

References

Adler, R.F., Sapiano, M.R.P., Huffman, G.J., Wang, J.-J., Gu, G., Bolvin, D., Chiu, L., Schneider, U., Becker, A., Nelkin, E., Xie, P., Ferraro, R., Shin, D.-B., 2018. The Global Precipitation Climatology Project (GPCP) monthly analysis (New Version 2.3) and a review of 2017 global precipitatioN. Atmosphere 9, 138.

Arabsahebi, R., Voosoghi, B., Tourian, M.J., 2018. An estimation of tropospheric corrections using GPS and synoptic data: improving Urmia Lake water level time series from Jason-2 and SARAL/AltiKa satellite altimetry. Adv. Space Res. 61, 2406–2417.

Chen, W., Liu, Y., Zhang, G., Yang, K., Zhou, T., Wang, J., Shum, C., 2022. What controls lake contraction and then expansion in Tibetan Plateau's endorheic basin over the past half century? Geophys. Res. Lett. 49, e2022GL101200.

Chen, X., 2022. The Theory and Methodology of Detecting Seasonal Lake Area Variations in the Tibetan Plateau With Deep Learning. Southern University of Science and Technology, Master's Thesis.

Gronewold, A.D., Stow, C.A., 2014. Water loss from the great lakes. Science 343, 1084–1085.

Hersbach, H., Bell, B., Berrisford, P., Biavati, G., Horányi, A., Muñoz Sabater, J., Nicolas, J., Peubey, C., Radu, R., Rozum, I., 2018. ERA5 hourly data on single levels from 1979 to present. In: Copernicus Climate Change Service (c3s) climate Data Store (cds) 10.

Huang, Q., Long, D., Du, M., Zeng, C., Li, X., Hou, A., Hong, Y., 2018. An improved approach to monitoring Brahmaputra River water levels using retracked altimetry data. Remote Sens. Environ. 211, 112–128.

Jiang, Y., Yang, K., Qi, Y., Zhou, X., He, J., Lu, H., Li, Xin, Chen, Y., Li, Xiaodong, Zhou, B., Mamtimin, A., Shao, C., Ma, X., Tian, J., Zhou, J., 2023. TPHiPr: a long-term (1979–2020) high-accuracy precipitation dataset (1/30°, daily) for the third pole region based on high-resolution atmospheric modeling and dense observations. Earth Syst. Sci. Data 15, 621–638.

Landerer, F.W., Flechtner, F.M., Save, H., Webb, F.H., Bandikova, T., Bertiger, W.I., Bettadpur, S.V., Byun, S.H., Dahle, C., Dobslaw, H., Fahnestock, E., Harvey, N., Kang, Z., Kruizinga, G.L.H., Loomis, B.D., McCullough, C., Murböck, M., Nagel, P., Paik, M., Pie, N., Poole, S., Strekalov, D., Tamisiea, M.E., Wang, F., Watkins, M.M., Wen, H.-Y.,

Wiese, D.N., Yuan, D.-N., 2020. Extending the global mass change data record: GRACE follow-on instrument and science data performance. Geophys. Res. Lett. 47 (12).
Li, J., Zeng, Q., 2003. A new monsoon index and the geographical distribution of the global monsoons. Adv. Atmos. Sci. 20, 299–302.
Li, K., Wang, J., Cheng, W., Wang, Y., Zhou, Y., Altansukh, O., 2022. Deep learning empowers the sne for automated water extraction in the Lake Baikal Basin. Int. J. Appl. Earth Obs. Geoinf. 112, 102928.
Li, L., Yan, Z., Shen, Q., Cheng, G., Gao, L., Zhang, B., 2019. Water body extraction from very high spatial resolution remote sensing data based on fully convolutional networks. Remote Sens. 11, 1062.
Liu, W., Chen, X., Ran, J., Liu, L., Wang, Q., Xin, L., Li, G., 2020. LaeNet: a novel lightweight multitask CNN for automatically extracting lake area and shoreline from remote sensing images. Remote Sens. 13, 56.
Ma, R., Yang, G., Duan, H., Jiang, J., Wang, S., Feng, X., Li, A., Kong, F., Xue, B., Wu, J., 2011. China's lakes at present: number, area and spatial distribution. Sci. China Earth Sci. 54, 283–289.
Muñoz-Sabater, J., 2019. ERA5-Land hourly data from 1950 to present. In: Copernicus Climate Change Service (C3S) Climate Data Store (CDS).
Pekel, J.-F., Cottam, A., Gorelick, N., Belward, A.S., 2016. High-resolution mapping of global surface water and its long-term changes. Nature 540, 418–422.
Ran, J., Ditmar, P., Liu, L., Xiao, Y., Klees, R., Tang, X., 2021. Analysis and mitigation of biases in Greenland ice sheet mass balance trend estimates from GRACE mascon products. J. Geophys. Res. Solid Earth 126, e2020JB020880.
Rodell, M., Houser, P., Jambor, U., Gottschalck, J., Mitchell, K., Meng, C.-J., Arsenault, K., Cosgrove, B., Radakovich, J., Bosilovich, M., 2004. The global land data assimilation system. Bull. Am. Meteorol. Soc. 85, 381–394.
Schneider, T., 2001. Analysis of incomplete climate data: estimation of mean values and covariance matrices and imputation of missing values. J. Clim. 14, 853–871.
Shen, Y., Xiong, A., 2016. Validation and comparison of a new gauge-based precipitation analysis over mainland China. Int. J. Climatol. 36, 252–265.
Smith, L.C., Sheng, Y., MacDonald, G., Hinzman, L., 2005. Disappearing arctic lakes. Science 308, 1429.
Song, C., Huang, B., Ke, L., 2013. Modeling and analysis of lake water storage changes on the Tibetan Plateau using multi-mission satellite data. Remote Sens. Environ. 135, 25–35.
Tapley, B.D., Watkins, M.M., Flechtner, F., Reigber, C., Bettadpur, S., Rodell, M., Sasgen, I., Famiglietti, J.S., Landerer, F.W., Chambers, D.P., Reager, J.T., Gardner, A.S., Save, H., Ivins, E.R., Swenson, S.C., Boening, C., Dahle, C., Wiese, D.N., Dobslaw, H., Tamisiea, M.E., Velicogna, I., 2019. Contributions of GRACE to understanding climate change. Nat. Clim. Chang. 9 (5), 358–369.
Wan, W., Xiao, P., Feng, X., Li, H., Ma, R., Duan, H., Zhao, L., 2014. Monitoring lake changes of Qinghai-Tibetan Plateau over the past 30 years using satellite remote sensing data. Chin. Sci. Bull. 59, 1021–1035.
Wang, J., Wang, L., Li, M., Zhu, L., Li, X., 2022. Lake volume variation in the endorheic basin of the Tibetan Plateau from 1989 to 2019. Sci. Data 9, 611.
Wang, Q., Yi, S., Sun, W., 2016. The changing pattern of lake and its contribution to increased mass in the Tibetan Plateau derived from GRACE and ICESat data. Geophys. J. Int. 207, 528–541.
Watkins, M.M., Wiese, D.N., Yuan, D.N., Boening, C., Landerer, F.W., 2015. Improved methods for observing Earth's time variable mass distribution with GRACE using spherical cap mascons. J. Geophys. Res. Solid Earth 120, 2648–2671.
Weng, L., Xu, Y., Xia, M., Zhang, Y., Liu, J., Xu, Y., 2020. Water areas segmentation from remote sensing images using a separable residual segnet network. ISPRS Int. J. Geo-Inf. 9, 256.
Wiese, D.N., Landerer, F.W., Watkins, M.M., 2016. Quantifying and reducing leakage errors in the JPL RL05M GRACE mascon solution. Water Resour. Res. 52, 7490–7502.
Xu, F., Zhang, G., Yi, S., Chen, W., 2022. Seasonal trends and cycles of lake-level variations over the Tibetan Plateau using multi-sensor altimetry data. J. Hydrol. 604, 127251.
Yao, F., Wang, J., Wang, C., Crétaux, J.-F., 2019. Constructing long-term high-frequency time series of global lake and reservoir areas using Landsat imagery. Remote Sens. Environ. 232, 111210.
Yao, F., Livneh, B., Rajagopalan, B., Wang, J., Crétaux, J.F., Wada, Y., Berge-Nguyen, M., 2023. Satellites reveal widespread decline in global lake water storage. Science 380 (6646), 743–749.
Yommy, A.S., Liu, R., Wu, S., 2015. SAR image despeckling using refined Lee filter. In: 2015 7th International Conference on Intelligent Human-machine Systems and Cybernetics. IEEE, pp. 260–265.
Yuan, X., Sarma, V., 2010. Automatic urban water-body detection and segmentation from sparse ALSM data via spatially constrained model-driven clustering. IEEE Geosci. Remote Sens. Lett. 8, 73–77.
Zhang, G., 2022. In: Center, N.T.P.T.P.E.D. (Ed.), The Lakes Larger Than 1km^2 in Tibetan Plateau (v3.1) (1970s-2022). National Tibetan Plateau/Third Pole Environment Data Center.
Zhang, G., Xie, H., Kang, S., Yi, D., Ackley, S.F., 2011. Monitoring lake level changes on the Tibetan Plateau using ICESat altimetry data (2003–2009). Remote Sens. Environ. 115, 1733–1742.
Zhang, G., Yao, T., Shum, C., Yi, S., Yang, K., Xie, H., Feng, W., Bolch, T., Wang, L., Behrangi, A., 2017. Lake volume and groundwater storage variations in Tibetan Plateau's endorheic basin. Geophys. Res. Lett. 44, 5550–5560.
Zhang, G., Luo, W., Chen, W., Zheng, G., 2019. A robust but variable lake expansion on the Tibetan Plateau. Sci. Bull. 64, 1306–1309.
Zhang, G., Yao, T., Xie, H., Yang, K., Zhu, L., Shum, C., Bolch, T., Yi, S., Allen, S., Jiang, L., 2020. Response of Tibetan Plateau lakes to climate change: trends, patterns, and mechanisms. Earth Sci. Rev. 208, 103269.
Zhang, J., Liu, P., Zhang, F., Song, Q., 2018. CloudNet: ground-based cloud classification with deep convolutional neural network. Geophys. Res. Lett. 45, 8665–8672.
Zhao, R., Fu, P., Zhou, Y., Xiao, X., Grebby, S., Zhang, G., Dong, J., 2022. Annual 30-m big Lake maps of the Tibetan Plateau in 1991–2018. Sci. Data 9, 164.